Applied Catalysis A: General 505 (2015) 105–115

Contents lists available at ScienceDirect

Applied Catalysis A: General

journal homepage: www.elsevier.com/locate/apcata

Controlling coke deactivation and cracking selectivity of MFI zeolite by H_3PO_4 or KOH modification

Eva Epelde[a,b], José I. Santos[c], Pierre Florian[d,e], Andrés T. Aguayo[a], Ana G. Gayubo[a], Javier Bilbao[a], Pedro Castaño[a,*]

[a] Chemical Engineering Department, University of the Basque Country (UPV/EHU), PO Box 644, 48080, Bilbao, Spain
[b] Department of Innovation and School Administration, Faculty of Psychology and Education, University of Deusto, PO Box 1, Bilbao 48080, Spain
[c] NMR Service, SGIKER, University of the Basque Country (UPV/EHU), "Joxe Mari Korta" Center, Tolosa Hiribidea, 72, 20018 San Sebastian, Spain
[d] CNRS, UPR3079CEMHTI, 1D Avenue de la Recherche Scientifique, 45071 Orléans Cedex 2, France
[e] Université d'Orléans, Avenue du Parc Floral, BP 6749, 45067 Orléans Cedex 2, France

ARTICLE INFO

Article history:
Received 4 June 2015
Received in revised form 14 July 2015
Accepted 15 July 2015
Available online 26 July 2015

Keywords:
ZSM-5 zeolite
Acidity modification
Oligomerization-cracking
Propylene
Coke deactivation

ABSTRACT

The effect of the basic (KOH) or acid (H_3PO_4) treatment of the MFI (HZSM-5) zeolite has been studied comparing the structural and acidic features with the catalytic performance and deactivation of a set of unmodified and modified zeolites (SiO_2/Al_2O_3 = 30–280, 0–3 wt% of K or P). The properties of the catalysts have been elucidated using XRD, ^{27}Al and ^{29}Si NMR, N_2 adsorption–desorption, and adsorption-TPD of tert-butylamine. The catalytic performance has been evaluated in the cracking of 1-butene by means of initial, 5 h on-stream activity and coke formation. Our results point to the fact that using zeolites with high SiO_2/Al_2O_3 ratio or neutralizing the strongest acid sites with KOH or H_3PO_4 increases propylene selectivity while decreases 1-butene conversion. The overall pathway of reaction involves propylene and other olefins as primary products that condensate in further steps to aromatics and ultimately to coke. This pathway can be controlled with less severe acidic features and by desilication with KOH or H_3PO_4 (particularly with the former).

1. Introduction

Acidic MFI zeolite (H-ZSM-5 or HZSM-5) is widely used for multiple processes linked with catalysis, adsorption and separation, in both conventional and sustainable refining concepts. The outstanding performance of MFI zeolite is attributed to its unique acid and structural features, which enable shape- and acid-selective reactions to occur. Furthermore, its porous network, of high connectivity, allows a very high surface-to-mass ratio and enhances mass transfer by favoring the outward diffusion of deactivating promoters [1–3]. The catalytic processes using MFI zeolite include (i) fluid catalytic cracking (FCC), (ii) methanol to hydrocarbons (MTH) or to olefins (MTO), (iii) bioethanol or bio-oil catalytic transformation, (iv) valorization of polyolefinic plastic wastes, and (v) interconversion of light olefins (ethylene or butene) into propylene. Indeed, MFI zeolite has very attractive shape selectivity for producing light olefins, and propylene in particular. Rahimi and Karimzadeh [4] have reviewed the main modifications of MFI zeolites for obtaining and intensifying light olefin production, since the structure and acidity of the MFI zeolite could be tuned for each specific application by properly selecting the SiO_2/Al_2O_3 ratio [5–7], calcination with different protocols [8], using vapor at high temperatures namely *steaming* [9,10], incorporating rare earth or transition metals [4,11,12], protons by cations like Na^+ [13], selecting a proper matrix of binders and fillers [14], and by treatment with acids or bases [15,16], among others.

Modification of MFI zeolite with H_3PO_4 is a very extended method for modifying framework tetrahedral Al (FAl^{IV}) of the zeolite, which is associated to the acid sites, and micropore blockage [17], with the sequential transformation of framework tetrahedral (FAl^{IV}) sites into (1) distorted tetrahedral (DAl^{IV}), (2) framework pentahedral (FAl^{V}), and (3) extra framework octahedral ($EFAl^{VI}$) [18,19]. These transformations are observed by solid state ^{29}Al MAS NMR in 1D or 2D [20]. When the degree of distortion is low, modifications could be restored by washing with hot water [17,21,22]. Besides the removal of FAl^{IV}, H_3PO_4 neutralizes Brönsted acidic sites with POH groups, particularly the strongest acid sites [23].

Modification of MFI zeolite with KOH implicates two different distortion pathways: (1) desilication by the alkali media [15] and (2) neutralization of acid sites by ion exchange with K^+ [24].

* Corresponding author.
E-mail address: pedro.castano@ehu.es (P. Castaño).

http://dx.doi.org/10.1016/j.apcata.2015.07.022

Despite the relatively scarce literature on this type of modifier, we have recently shown that this treatment notably reduces total acidity and homogenizes acid strength [25]. The treatment with alkali generates mesopores and hierarchical structures by desilication [26,27], which facilitate the diffusion of the compounds of the reaction medium and decrease the amount of strong acid sites [28]. Moreover, alkali can also reacts with Al sites [29]. Katikaneni et al. [24] modified MFI zeolite using aqueous solutions of KCO_3 finding that K^+ decreased not only the acid site strength but also the total acidity of the catalyst. In the case of the catalyst containing 2 wt% of K, there was a complete neutralization of the strong acid sites.

As KOH and H_3PO_4 react with FAl^{IV} and FSi^{IV}, the acidity and crystal size of the zeolite may decrease. In fact, the reduction of crystal size decreases the residence time of olefins within the interior of the zeolite micropores [30] as well as the proportion of bimolecular reactions, particularly hydrogen transfer. As a result, the catalytic deactivation by coke is decreased. In addition, KOH and H_3PO_4 reacts preferentially with the strongest acid sites, inhibiting the participation of these sites in the condensation of coke precursors and attenuating deactivation [25,31]. It is also well established in the literature the increase in hydrothermal stability of MFI zeolite after P modification [16,32]. Other methods for controlling coke deactivation include agglomeration with different binders and fillers [33], or incorporating the zeolite in a composite [14]. These methods target the minimization of coke deposition in the entrance or within the micropores of the zeolite by adding mesopores that "arrest" coke outside the zeolite.

The interconversion of light olefins (ethylene or butenes) into propylene is a suitable process for using K- and P-modified zeolites. Propylene demand is increasing 5.7% every year, whereas this product is used for producing polypropylene, propylene oxide and acrylonytrile, among others [34]. According to the forecasted increase in ethylene production by steam cracking [35], propylene will be produced only in other catalytic processes, in which its selectivity is low. Within this scenario, light olefin interconversion is attractive for adjusting its production to market prices and demands. The demand for butene stream is lower than that for ethylene and propylene, especially due to the decrease in the production of methyl tert-buthyl ether (MtBE) as additive for gasoline. In addition, the transformation of 1-butene into other more interesting light olefins is an alternative to the oligomerization for the production of middle distillates [36]. The literature reports the complexity of the 1-butene cracking reaction scheme (including oligomerization-cracking, dehydrogenation-aromatization and hydrogen transfer reactions) [37,38] and the significant effect of MFI zeolite properties on product distribution and stability [5,31,39]. Lin et al. [40] proposed several reaction pathways for the catalytic cracking of 1-butene on MFI zeolites and established an optimum amount of acid sites (0.181 mmol g^{-1}) in order to achieve high propylene selectivity. Koyama et al. [41] investigated the role of the pore volume of zeolites with 8-, 10- and 12-membered rings for the selective production of propylene from other olefins, by determining the optimum zeolite cavity volume (152–223 $Å^3$) for the formation of the octylcarbenium ion which produces propylene. Furthermore, the local Al distribution in the MFI framework affects the product composition during olefin cracking [39].

Determining the strength of the correlation between the catalytic features and its intrinsic performance (activity, conversion, yields, selectivity and deactivation among others) is a crucial step to rationally design catalysts or evaluate kinetic parameters. This is done by a sensitivity analysis, which is a preliminary step before the regression analysis of the data with a model [42]. This protocol has been successfully applied to evaluate kinetic parameters during the cracking of hydrocarbons [43] and could be useful for understanding the effect of acidity in the cracking and deactivation mechanisms [44]. The present work investigates the relationship between the structure, acidity and performance of the MFI zeolite (SiO_2/Al_2O_3 = 30–280, unmodified and modified with KOH or H_3PO_4) in the transformation of 1-butene. We have synthesized 9 zeolites, characterized them by XRD, ^{27}Al and ^{29}Si NMR, N_2 adsorption–desorption, adsorption-TPD of tert-butylamine, and then agglomerated with bentonite and alumina to be used in a fixed-bed reactor. A preliminary performance-testing revealed the suitability of less acidic zeolite (SiO_2/Al_2O_3 = 280), which strikes a suitable balance between 1-butene conversion, propylene selectivity and catalyst stability, and hence, we performed a sensitivity and regression analysis correlating the key features of the zeolite that govern selectivity and deactivation.

2. Experimental

2.1. Catalyst preparation

Catalysts were prepared based on commercial MFI zeolites of different SiO_2/Al_2O_3 ratio, supplied in ammonium form by Zeolyst International: 30 (CBV 3024E), 80 (CBV 8014) and 280 (CBV 28014). The zeolite acid forms (named HZ) were obtained by calcination at 570 °C for 2 h, whereas the modified ones (1 and 3 wt% of K or P) were prepared by incipient wetness impregnation at 70 °C under vacuum in a BÜCHI R-114 rotovapor using known amounts of KOH (85% purity, Panreac) or H_3PO_4 (85% purity, Merck) solutions, respectively. Modified zeolites are named according to the nominal content of the modifier (1K, 3K, 1P or 3P) followed by the corresponding SiO_2/Al_2O_3 ratio, so the catalysts are: HZ30, 1K30, HZ80, 1K80, HZ280, 1K280, 3K280, 1P280 and 3P280.

The catalysts were obtained by agglomerating each zeolite (25 wt%) with bentonite (Exaloid, 30 wt%) as binder and alumina (Martinswek, calcined at 1000 °C, 45 wt%) as inert charge. The catalyst particles were obtained by wet extrusion, then sieved to a particle diameter between 0.3 and 0.15 mm, dried in an oven at 110 °C for 24 h and calcined at 570 °C for 2 h. After agglomeration a matrix with a meso and macroporous structure embedding the zeolite crystals is generated, so as to [45,46]: (i) provide the catalyst with a high mechanical resistance for its use in a fixed or fluidized bed reactor; (ii) improve accessibility of the reaction medium compounds to the zeolite crystals; (iii) facilitate the deposition of coke in the meso and macroporous matrix, and; (iv) favor heat dissipation in the particle during the regeneration step by coke combustion, thus increasing hydrothermal stability.

2.2. Catalyst characterization

The content of K or P was determined by ICP-AES in a Jobin Yvon (ACTIVA) spectrometer. X-ray diffraction (XRD) patterns at room temperature were obtained in a PAN alytical Xpert PRO difractometer equipped with CuKα radiation of 1.5418 Å. The patterns were recorded using a 2θ step of 0.026° in the 6–60° range. The FULLPROF program was used to perform the profile refinement of the diffractogram without structural model (pattern matching routine). This procedure was carried out using the peak-fit option of the WinPLOTR program without structural model. The simulated profiles were then used to recalculate the starting unit cell parameters from the 2θ peak positions. The coherent diffraction crystal size (d_c) was determined by using Scherrer equation referred to the deconvolution of the diffraction peaks observed between 7–10°. An example of the full-profile refinement is shown in Fig. S1 of the Supplementary material.

Solid-state ^{29}Si and ^{27}Al NMR spectra were recorded on a Bruker 400 AVANCE III WB spectrometer (9.40 T) under magic angle spinning (MAS) at the resonance frequency of 79.49 and 104.27 MHz, respectively. Solid-state ^{29}Si NMR spectra recorded with a spinning

rate 10 kHz. Cross-polarization measurements were done using a 90° pulse for protons of 3.40 μs, 2.0 ms of contact time, and 5 s of recycle delay. Solid-state ^{27}Al NMR spectra recorded with a spinning rate 10 kHz and a pulse length of 14 μs with a 1.0 s repetition time. The zeolites were packed into a cylindrical zirconia rotor (4 mm external diameter). The ^{29}Si and ^{27}Al chemical shifts are given relative to tetramethylsilane and $Al(NO)_3$ respectively. Examples of ^{29}Si and ^{27}Al NMR deconvolution are given in Fig. S2 of the Supplementary material. It is important to indicate that ^{29}Si NMR spectra have been obtained using CP-MAS methodology, in which protons transfer polarization to Si. Thus, the values of ^{29}Si NMR spectral deconvolution cannot be used quantitatively as they depend upon the proximity and number of protons located nearby Si. For a given catalyst it is to be expected that Q_4 is being underestimated with respect to Q_3. However, as all the catalysts have been analyzed in the same experimental setup, the trend of the Q_3/Q_4 ratio among them is true.

The physical properties were measured by N_2 adsorption–desorption (Micromeritics ASAP 2010). The experimental procedure for determining physical properties consists of degasifying the zeolite at 150 °C and under vacuum (10^{-3} mmHg) for 8 h, in order to remove possible impurities, followed by N_2 adsorption–desorption in multiple equilibrium steps until zeolite saturation at the −196 °C temperature.

The total acidity and acid strength distribution of the catalysts have been determined by monitoring the adsorption–desorption of tert-butylamine (t-BA), by combining the techniques of thermogravimetric analysis and differential scanning calorimetry during the adsorption of the base at 150 °C. The total acidity is quantified as the amount of the base chemisorbed at 150 °C [25,45], in $mmol_{t\text{-}BA}\ (g_{zeolite})^{-1}$, whereas the acid strength is defined as the heat released during the adsorption of the base, $kJ\,(mol_{t\text{-}BA})^{-1}$. A very comprehensive review of the characterization of the number of acids sites and acid strength can be found elsewhere [47].

Catalyst saturation at 150 °C is followed by temperature programmed desorption (TPD) (at 5 °C min^{-1} up to 550 °C) using a Setaram TG–DSC calorimeter connected on-line with a Thermostar mass spectrometer from Balzers Instruments [45]. The TPD of amines is based on the formation of alkyl ammonium ions (from adsorbed alkyl amines protonated by Brönsted sites), which undergo cracking to give ammonia and olefins in a well-defined temperature range via a reaction similar to the Hofmann-elimination reaction [48]. Above 150 °C t-BA is cracked on the acid sites releasing butene, whose signal (m/z = 56) is monitored by mass spectrometer, thereby identifying sites of enough acidity for cracking. The temperature of maximum desorption-cracking of t-BA (T_{TBA}) is linked to the acid strength of the catalyst, as stronger acid sites are active for the cracking of t-BA at lower temperatures. Considering this, the lower the temperature of the peak (lower T_{TBA}), the higher the acid strength of the sites, which is the opposite effect to that observed in the TPD analysis of commonly used NH_3 [6]. Besides, a small fraction of t-BA (signal at m/z = 58) is desorbed without cracking, corresponding to the base physisorbed on weak acid sites, which are inactive for the cracking of t-BA, and consequently also for the reactions involved in the transformation of 1-butene [25,45].

Moreover, the interest of using this base is noteworthy since t-BA allows a greater sensitivity in the thermo-gravimetric measurement of the base (due to its higher molecular weight) than NH_3. This sensitivity is required for determining rigorously the differential adsorption heat of the base, especially for catalysts of moderate acid strength as some of the samples studied in this work.

The coke content deposited on the catalysts was determined by temperature-programmed oxidation (TPO) in a SDT 2960 thermobalance (TA Instruments). After stabilization of the zeolite at 250 °C for 30 min in a He stream, the oxidant mixture (25 vol% O_2 in He) was introduced and the combustion took place by following a heating ramp of 8 °C min^{-1} up to 600 °C, and this temperature was maintained for 1 h to complete coke combustion.

2.3. Reaction equipment and product analysis

The runs have been carried out under atmospheric pressure in an automated reaction device (Microactivity of PID Eng&Tech, Madrid, Spain) equipped with an isothermal fixed-bed reactor (of 316 stainless steel with an internal diameter of 9 mm and 10 cm of effective length) and a micro-GC Agilent 3000A for online analysis of the reaction products, which has been described in detail in a previous work [25]. The micro-GC, with Soprane software, is provided with 4 analytical modules and the following columns: a molecular sieve (MS-5A, 10 m) for analysis of CH_4; Porapak Q (PPQ, 8 m), for C_2–C_3 light olefins; Alumina (10 m), for C_2-C_5 light paraffins and olefins, and; OV-1, for C_5–C_{10} fraction and aromatics BTX. Product stream is analyzed every 4 min. The quantification and identification of the compounds is carried out based on calibration standards of known concentration. The balance of atoms (C and H) is higher than 98 wt% in all runs. For this balance we have included the formation of products that are negligible in terms of overall yields, but important in terms of H (hydrogen and methane) and C (coke) atomic proportion.

Experiments have been carried out under the following operating conditions: total pressure, 1.5 bar (small overpressure to account for the pressure drop in the fixed bed reactor and the device for continuous sampling); 500 °C; space time, 1.6 ($g_{catalyst}$ h) $(mol_C)^{-1}$; WHSV, 8.75 h^{-1}; 1-butene (99 vol%, Air liquide) partial pressure in the feed, 1.35 bar; time on stream, 5 h. Blank runs (without catalyst) were carried out to confirm that thermal cracking is insignificant below 550 °C. The reaction indices studied have been: (i) butene conversion, and, (ii) selectivity of each lump of products (C_2H_4, C_3H_6, C_2–C_4 paraffins, C_{5+} aliphatics and aromatics BTX). It should be mentioned that methane, hydrogen and coke selectivities are lower than 1% under the operating conditions studied, thus their corresponding lumps of products have been omitted for further discussion.

Conversion has been defined as follows:

$$X = \frac{F_0 - F}{F} \quad (1)$$

where F_0 is the molar flow rate of 1-butene in the feed and F is the flow rate of butenes (in thermodynamic equilibrium) in the outlet stream, with both terms being expressed in C atoms contained.

The selectivity is:

$$S_i = \frac{F_i}{F_0 - F} \times 100 \quad (2)$$

where F_i is the molar flow-rate of the i lump in the product stream expressed in C-atom content.

3. Results

3.1. Catalyst properties

The results of the elemental analysis shown in Table 1 ratify that the contents of K and P are approximately 1 or 3 wt% for the modified zeolites. XRD patterns for the unmodified and K or P modified zeolites are displayed in Fig. 1. These patterns show the characteristic peaks of MFI zeolite (Pnma, N°62). The coherent diffraction crystal size (d_c, Table 1) has been calculated using the Scherrer equation, which could have limitation for zeolites with different crystal shapes [49]. Nevertheless the reported values of d_c in Table 1 correspond to unmodified and modified zeolites of the same parent one (HZ280) so that the shape of the crystal will

Table 1
Properties of the fresh zeolites.

Zeolites	K or P (wt%)	d_c [b] (nm)	S_{BET} ($m^2\ g^{-1}$)	$V_{P/P0=0.2}$ [a] ($cm^3\ g^{-1}$)	acidity ($mmol\ g^{-1}$)	strength ($kJ\ mol_{t\text{-}BA}^{-1}$)	T_{TBA} [c] (°C)
HZ30	0	–	448	135	0.67	150	196
1K30	0.92	–	434	130	0.59	110	222
HZ80	0	–	556	170	0.42	145	200
1K80	0.93	–	456	140	0.38	85	235
HZ280	0	140 ± 13	512	144	0.15	120	210
1K280	0.78	70 ± 7	415	121	0.13	75	236
3K280	2.75	35 ± 3	235	68	0.09	57	247
1P280	0.97	75 ± 7	322	126	0.15	118	222
3P280	3.21	60 ± 6	365	95	0.14	115	232

[a] Volume of N_2 adsorbed at $P/P_0 = 0.2$.
[b] Average crystal particle size according to XRD.
[c] Temperature of maximum t-BA desorption-cracking rate.

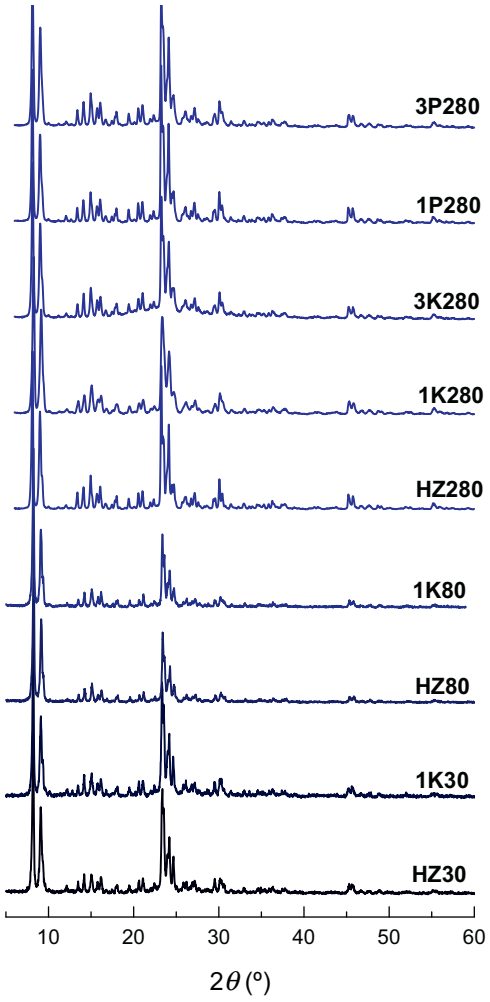

Fig. 1. XRD patterns of the unmodified and modified MFI zeolites.

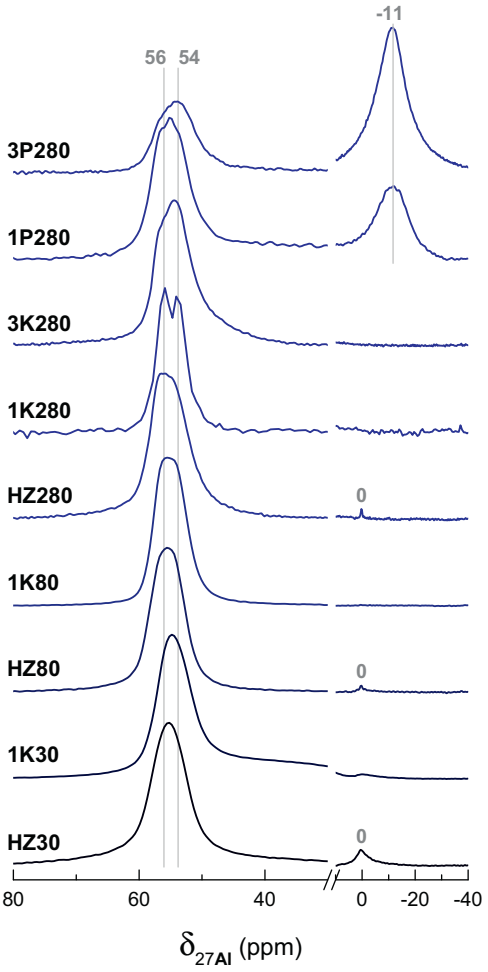

Fig. 2. ^{27}Al NMR profiles of the unmodified and modified MFI zeolites.

not vary significantly. Indeed, some authors have found a correlation of the values of d_c calculated using the Scherrer equation and transmission electron microscopy (TEM) [50]. The reported errors of d_c on Table 1 have been calculated assuming different shapes of the zeolite crystals. Attending to the results of d_c for catalyst with initial $SiO_2/Al_2O_3 = 280$, it can be deduced that modifying with 1 wt% of K or P decrease the size of the crystals from 140 down to ~70–75 nm, and higher modification with K or P leads to further decrease of crystal size. Xue et al. [23] have found relatively similar results upon the modification with H_3PO_4 of MFI zeolite.

Fig. 2 shows the ^{27}Al MAS NMR spectra of the modified and unmodified zeolites. The spectrum of unmodified zeolites HZ30, HZ80 and HZ280 consists of an intense signal at *ca.* 55 ppm corresponding to framework tetrahedral Al (FAl^{IV}) comprising the zeolite structure, and another weaker signal at 0 ppm associated to extra-framework octahedral Al ($EFAl^{VI}$) [17], formed during calcination [51]. HZ30 and 1K30 show a higher value of the base line at 38 ppm corresponding to framework penta-coordinated FAl^{V} sites, typically found in zeolites with high concentration of Al [52]. Nonetheless, these types of FAl^{V} sites do not correspond to highly acidic ones, which are normally associated with FAl^{IV} and $EFAl^{VI}$ sites. As previously reported, the modification procedure

Table 2
^{27}Al NMR peak deconvolution of the fresh zeolites.

Zeolites	P-EFAl^{VI} (−11 ppm)	EFAl^{VI} (0 ppm)	FAl^{V} (38 ppm)	FAl^{IV-54} (54 ppm)	FAl^{IV-57} (57 ppm)	FAl^{IV-54}/ FAl^{IV-57}
HZ30	0	2.3	10.6	52.4	34.7	0.663
1K30	0	0	14.9	71.2	13.9	0.195
HZ80	0	1.8	0	49.3	48.9	0.992
1K80	0	0	0	69.6	30.4	0.437
HZ280	0	0.8	0	63.4	35.8	0.565
1K280	0	0	0	75.8	24.2	0.319
3K280	0	0	0	88	12	0.136
1P280	50.8	0	0	36.6	12.7	0.346
3P280	81.5	0	0	17	1.5	0.088

with water (in this case present with KOH and H_3PO_4) removes EFAl^{VI} sites along the zeolite [16,53]. P-modified MFI zeolites show another peak at −11 ppm corresponding to P-coordinated extra-framework octahedral Al (P-EFAl^{VI}) [54]. This band is very broad, indicating a low symmetry and poor crystallinity of P-EFAl^{VI} species [53]. Our results of P-modified zeolites show only Al^{IV} and Al^{VI} coordination, which are poles of a transition through Al^{V} [18,55].

The FAl^{IV} has been deconvoluted in two tetrahedral sub-bands: FAl^{IV-57} at 57 ± 0.5 ppm and FAl^{IV-54} at 54 ± 0.5 ppm. These chemical shift (δ_{Al}) corresponds to bond angles (α) of the tetrahedral T–O–T of 150° (FAl^{IV-57}) y 157° (FAl^{IV-54}) according to the following equation [9]:

$$\delta_{Al} = 132 - 0.5\alpha \quad (3)$$

Interestingly, Kučera and Nachtigall [56] have proved that this correlation does no hold for high-siliceous zeolites. Based on these assumptions, the ^{27}Al MAS NMR spectra of the catalyst have been deconvoluted in 5 lorentzian peaks with fixed positions: −11, 0, 38, 54 and 57 ppm. The results of the deconvolution are summarized in Table 2. The amount of EFAl^{VI} sites decrease with the increase of SiO_2/Al_2O_3 while FAl^{V} are only observed for HZ30 and 1K30, as previously explained.

Ong et al. [9] demonstrated that FAl^{IV-57} with angles of 150° corresponds to accessible Al sites whereas FAl^{IV-54} with angles of 157° corresponds to internal and inaccessible Al sites on MFI zeolites. Maier et al. [57] supported this hypothesis on BEA zeolite. On the other hand, Sarv et al. [58] have correlated FAl^{IV-57} with weak Brönsted acids sites and FAl^{IV-54} with stronger ones of the MFI zeolite. Our results (Table 2) show that the ratio of FAl^{IV-57}/FAl^{IV-54} sites decrease severely upon the treatment with 1K for the zeolites: 71, 56 and 43% for HZ30, HZ80 and HZ280 catalysts, respectively. The decrease of the ratio of FAl^{IV-57}/FAl^{IV-54} sites are comparable using P as compared with K, however, in the former modification an intense P-EFAl^{VI} is observed, accounting for the 51 and 81% for the 1P280 and 3P280 catalysts, respectively. Thus, our results support the assignment of the FAl^{IV-57} as accessible Al sites, made by the group of Lercher [9,57]: the treatments of K and P preferentially modify the more accessible Al sites and the extent of this modification increase for higher amounts of K and P.

Fig. 3 shows the ^{29}Si CP MAS NMR spectra of the zeolites. The spectra of zeolites show bands at −119.5, −112.9, −108.6, −104.5 ppm, and small shoulders at −97.7 and −93.6 ppm. The band at −119.5 ppm, can be univocally assigned to Q_4 coordination (Si(OSi)$_4$) sites which is present in almost all the zeolites, but particularly intense for the HZ280 zeolite. The bands at −112.9, −108.6 and −104.5 ppm cannot be univocally assigned as several coordination states of Si are present. Typically, Q_4 coordination (Si(OSi)$_3$(OAl)) sites appear 10 ppm higher than (Si(OSi)$_4$) [53], so that the −112.9 and −108.6 ppm bands of HZ30, 1K30, HZ80 and 1K80 can be ascribed to this type of coordination [55]. On the other hand, the bands at −112.9, −108.6 and −104.5 ppm appearing in the P280 and K280 modified zeolites cannot be correlated with Al

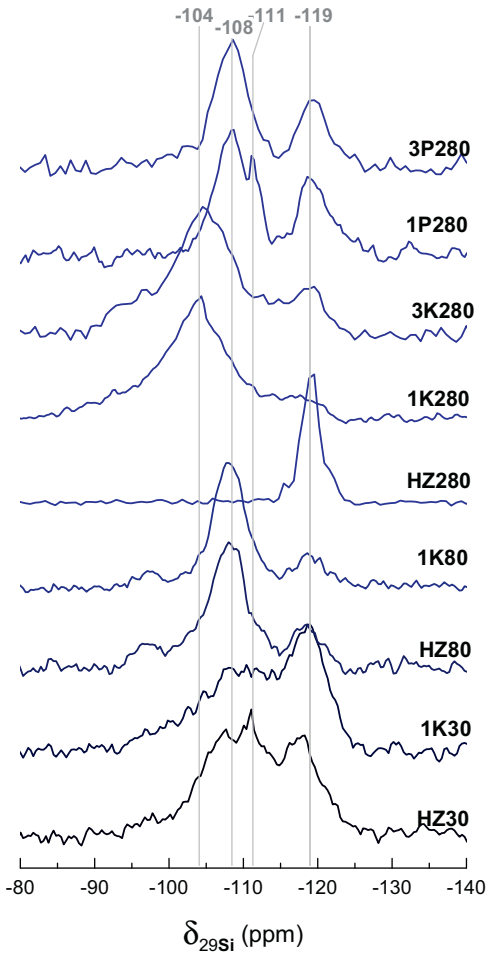

Fig. 3. ^{29}Si NMR profiles of the unmodified and modified MFI zeolites.

incorporation to the Si environment, as Al is being partially eliminated from the framework (Fig. 2). The bands at −112.9, −108.6 and −104.5 ppm for the P280 and K280 modified zeolites are assigned to Q_3 coordination (Si(OSi)$_3$(OH)) or silanol sites [59] interacting with K or P. The K280 modified zeolites have bands with higher chemical shifts than that of P280 modified ones, whereas the spectra remains approximately the same between HZ30-1K30 and HZ80-1K80, as previously reported for zeolites with low SiO_2/Al_2O_3 ratio [55]. This result is due to a higher interaction of K^+. The bands at −97.7 and −93.6 ppm are assigned to Q_2 coordination (Si(OSi)$_2$(OH)$_2$).

Our results point in the same direction than Zhuang et al. [55], who demonstrated that the treatment with H_3PO_4 of MFI zeolites produce simultaneous dealumination and desilication. H_3PO_4 seems to attack more efficiently Al sites, as proved in Fig. 2, whereas KOH seems to attack much more efficiently Si sites. For the calcula-

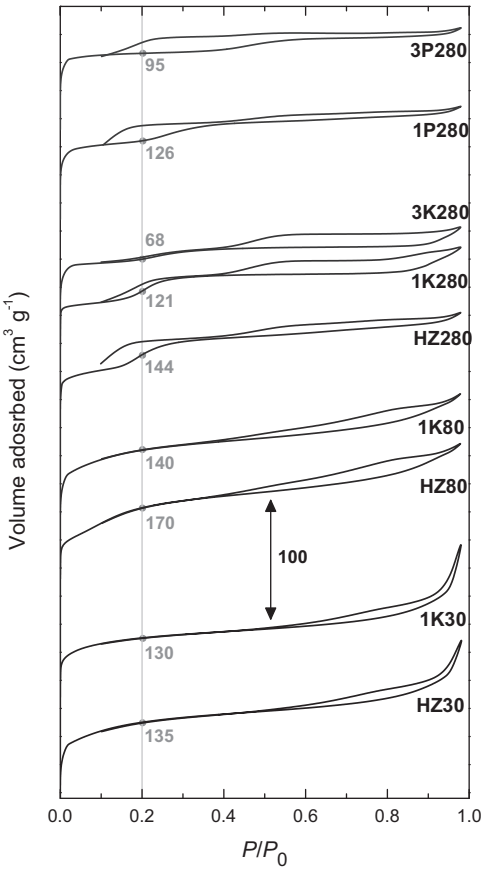

Fig. 4. Adsorption–desorption isotherms of N_2 on the unmodified and modified MFI zeolites. The values of adsorbed volume at $P/P_0 = 0.2$ ($V_{P/P0=0.2}$) have been represented for comparing the adsorption capacity of each catalyst.

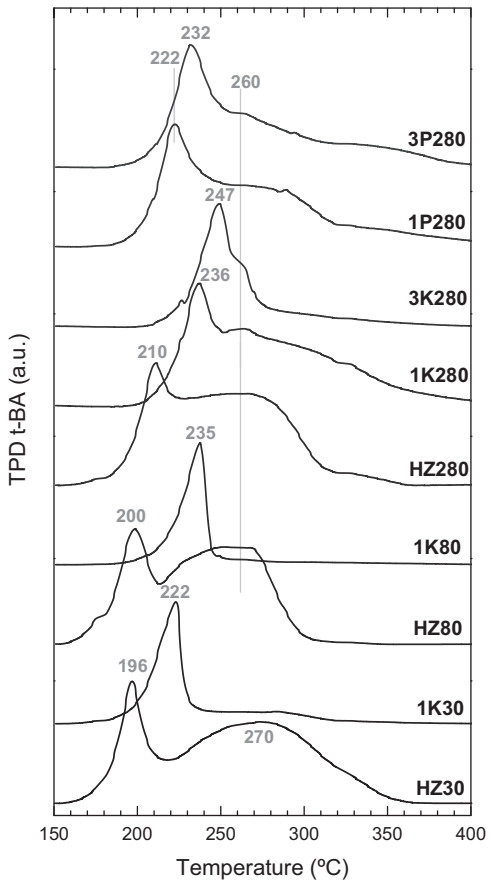

Fig. 5. Desorption of t-BA from the unmodified and modified MFI zeolites. The profiles have been normalized, the area under these profiles correspond to the total acidity, which is given in Table 1.

tion of the bond angle (α) from the chemical shift (δ_{Si}), the following expression has been proposed:

$$\delta_{Si} = -25.44 - 0.579\alpha \quad (4)$$

Whereas for highly siliceous HZSM-5 zeolite other empirical correlation has been proposed [60]:

$$\delta_{Si} = -11.90 - \frac{267.9\cos(\alpha)}{(\cos(\alpha) - 1)} \quad (5)$$

The lorentzian deconvolution of the ^{29}Si CP MAS NMR spectra has been summarized in Table 3. The treatment with 1 wt% K transforms Q_4 into Q_3 sites for all the zeolites, however this effect is more dramatic for the HZ280 catalyst.

Fig. 4 shows the N_2 adsorption–desorption isotherms for the zeolites studied and the intercept of volume at $P/P_0 = 0.2$ that is indirectly associated for the same type of catalysts to the micropore volume [61]. Adsorption branches of HZ30, 1K30, HZ80 and 1K80 zeolites correspond to type II materials, whereas the desorption hysteresis of the same zeolites corresponds to type H3. This behavior is typical of zeolites with micro and mesopores with slit shaped pores. The modification of the parent zeolite with 1 wt% of K, affects more significantly to the adsorption at $P/P_0 < 0.2$, thus to the micropores of the catalysts. The 280 family of unmodified and modified catalysts show two adsorption/hysteresis steps. The former step at $P/P_0 < 0.4$ indicates the existence of uniform pores of about 2 nm according to the model of BJH. Groen and Perez-Ramirez [62] have demonstrated that this is a result of a "phase transition of the adsorbed N_2 from a disordered fluid phase to a more ordered crystalline like phase and consequently do not indicate real mesoporosity", and this is due to a high homogeneity of the surface. Independently and interestingly, we observe a decrease of the fluid-to-crystalline transition (Fig. 4) upon the modification with increasing amounts of KOH or H_3PO_4. This results point to

Table 3
^{29}Si NMR peak deconvolution of the fresh zeolites.

Zeolites	Q_4 (−119.5 ppm)	Q_4 or Q_3 (−112.9 ppm)	Q_4 or Q_3 (−108.6 ppm)	Q_4 or Q_3 (−104.5 ppm)	Q_3 (−97.7 ppm)	Q_3 (−93.6 ppm)
HZ30	26.2	27.6	32.7	12.7	0.8	0
1K30	40.1	24.6	17.1	13.7	4.4	0
HZ80	14.5	0	62.5	17.2	5.8	0
1K80	12.9	0	76.6	8.5	2	0
HZ280	97.1	0	0.3	0.1	1.3	1.1
1K280	4.3	7.3	2.2	62	19.1	5.1
3K280	12.3	8.2	8.1	55	12.4	4.1
1P280	33	3.3	63.3	0.4	0	0
3P280	28.8	0	63.9	5.3	1.2	0.7

Table 4
Kinetic results at zero time on stream (in wt%).

Catalysts	X	$S_{ethylene}$	$S_{propylene}$	$S_{paraffins}$	S_{C5+}	S_{BTX}
HZ30	98.8	2.5	4.7	54.8	4.8	31.8
1K30	96.0	3.4	6.8	53.8	10.2	25.2
HZ80	91.6	6.0	9.5	43.0	16.4	24.5
1K80	85.0	7.2	19.4	36.1	26.3	10.7
HZ280	82.4	8.6	26.6	29.3	24.9	10.4
1K280	74.5	7.7	40.4	16.5	29.5	5.6
3K280	55.5	2.3	54.7	7.3	35	0.7
1P280	80.4	8.8	29.8	24.0	27.5	9.6
3P280	78.1	8.9	32.9	21.8	26.8	9.5

Table 5
Kinetic results after 5 h on stream (in wt%).

Catalysts	X	$S_{ethylene}$	$S_{propylene}$	$S_{paraffins}$	S_{C5+}	S_{BTX}	Coke[a]
HZ30	88.0	7.2	17.7	38.5	13.2	22.3	3.7
1K30	87.5	12.1	22.1	25.6	22.4	17.0	2.0
HZ-80	88.8	8.4	15.2	37.0	20.7	18.3	2.5
1K80	85.3	8.5	32.2	24.7	29.0	5.6	1.5
HZ280	77.5	8.9	30.9	25.8	25.2	9	1.3
1K280	71.1	5.5	46.2	11.6	33.4	3.1	1.1
3K280	38.5	1.3	53.9	6.0	38.0	0	0.9
1P280	78.4	9.3	35.7	20.3	28.5	5.3	1.2
3P280	76.7	9.0	37.8	19.8	28.8	4.4	1.0

[a] Referred to g of catalyst.

an increase of heterogeneity and imperfections for the modified zeolites with initial SiO_2/Al_2O_3 = 280.

The main physical properties of fresh zeolites are summarized in Table 1. The modification with P entails a drop in the BET surface area and pore volume, which is attributed to the blockage of the micropores by phosphorous [54,63]. Singularly, the same effects observed for the zeolites modified with K, where the decrease in micropore surface area is due to micropore blockage by K_2O [24] or the desilication affecting micropores by the alkali treatment [27]. This effect is more significant for high SiO_2/Al_2O_3 ratios and therefore, the latter explanation is more plausible. Indeed, the N_2 adsorption-desorption isotherms of the 280 catalyst family, upon the treatment of KOH and H_3PO_4, resemble the desilication and creation of mesopores in the silicalite-1 (all silica version of the HZSM-5 zeolite) [64]. The agglomerated final catalyst containing zeolite, bentonite and alumina provides with a three level porosity system with micro, meso and macropores: zeolites contribute to the micropores whereas the matrix contribute to the meso and macropores [65].

TPD of tert-butylamine (t-BA) profiles for unmodified and modified zeolites are plotted in Fig. 5. The acid properties (total acidity and average acid strength) are also summarized in Table 1. The unmodified HZ30 zeolite shows a main peak at 196 °C that corresponds to strong acid sites able to crack t-BA at this low temperature [25,45]. As the SiO_2/Al_2O_3 ratio is increased, the temperature required to crack t-BA increases; HZ80, 200 °C; and HZ280, 210 °C. Additionally, these unmodified zeolites show another broad band at 260–270 °C corresponding to weak acid sites that require higher temperature for cracking t-BA [25,66]. 1K30 and 1K80 modified zeolites display a unique peak at 222–247 °C corresponding to medium acid sites, whereas 280 modified zeolites show this peak and a shoulder of weak acid sites at 260 °C. The amount of acid sites (Table 1) notably decreases with increasing SiO_2/Al_2O_3 ratio (from 0.67 to 0.15 $mmol_{t\text{-}BA}\ g_{zeolite}^{-1}$ for HZ30 and HZ280, respectively), and by modification with KOH or H_3PO_4, especially by the former. The acid strength measured during the isothermal adsorption of t-BA is also decreased by the SiO_2/Al_2O_3 ratio or the modification extent (Table 1). And this trend correlates with the desorption temperature depicted in Fig. 5 and other observations in literature [13,25,67].

3.2. Catalysts performance

Table 4 shows the kinetic results at zero time on stream for all the catalysts studied. 1-butene conversion notably decreases with an increase in the SiO_2/Al_2O_3 ratio. However, an opposite trend is observed in propylene selectivity as zeolites with higher SiO_2/Al_2O_3 ratio enhances propylene selectivity from 4.7% for HZ30 catalyst to 26.6% for HZ280, as well as ethylene and C_{5+} fraction selectivity (which is mainly olefinic). Secondary reactions of aromatization and hydrogen transfer are catalyzed by strong acid sites and they are suppressed in high silica zeolites to some extent [40]. These reactions are involved in the formation of aromatics BTX and C_2–C_4 paraffins [68]. Ethylene selectivity is relatively lower than propylene selectivity, which allows obtaining a propylene/ethylene ratio of 3.1 in the case of HZ280 catalyst.

The modification with KOH is effective for notably increasing propylene selectivity, with this effect being more significant on zeolites with high SiO_2/Al_2O_3 ratio and high K contents [67], although this is at the expense of a decrease in conversion which drops down to 55.5% for 3K280. It should be mentioned that ethylene selectivity decreases with the K content of the catalyst.

The modification with H_3PO_4 decreases conversion while enhances propylene selectivity. This observation is similar to that for K, but less dramatic. Propylene selectivity increases more than 10% for 3 wt% compared to 1 wt% of P, with a slight decrease (−3%) in butene conversion. A more significant effect of P modification is reported in the literature for MFI zeolites of lower SiO_2/Al_2O_3 ratio (for values between 25 and 40) [21,63,69]. Dědeček et al. [70] and Sazama et al. [39] have indicated that the local distribution of Al in the framework has a significant effect on the side reactions. As FAl sites get closer to each other, bimolecular reactions as hydrogen transfer are enhanced. This observation indicates that independently of the method employed to decrease the amount of acid sites, the side reactions are weakened due to the decrease in the acid site density and their acid strength.

The kinetic results after 5 h on stream are summarized in Table 5. The selectivity of C_2–C_4 paraffins and BTX decreases throughout time on stream, whereas propylene, ethylene and C_{5+} fraction (mainly olefinic) selectivity increases in the same period (0–5 h). This decrease in C_2–C_4 paraffin and BTX selectivity is attributed to the drop of acidity when increasing TOS. In addition, it is well reported in the literature the role of C_2–C_4 paraffins and BTX as final products, while olefins (ethylene, propylene and C_{5+}) are intermediates in the reaction scheme of the 1-butene cracking [31,38].

Zeolites with higher SiO_2/Al_2O_3 ratio keep the activity and selectivity for longer time on stream, which in another words means that the catalyst is more stable. 1-butene conversion decreases 11% for HZ30 catalyst and 6% for HZ280 catalyst. The observed trend of catalyst stability is a consequence of the differences in coke deposition. The coke content determined by TG-TPO is shown in Table 5. Coke deposition is attenuated when the SiO_2/Al_2O_3 ratio is increased (3.7 wt% for HZ30 zeolite and only of 1.3 wt% for HZ280 zeolite) and for the most severely modified zeolites (3K and 3P).

Fig. 6 shows the selectivity of propylene and aromatics (BTX) for the different catalysts studied at TOS = 0 h (Fig. 6a) and 5 h (Fig. 6b). The latter graph contains also the coke content of the deactivated catalysts. Interestingly, the evolution of BTX selectivity increases at higher conversion values of 1-butene and this tendency occurs for the fresh and deactivated catalyst. This has been observed previously in Tables 4 and 5, however Fig. 6 reveals that there are unified tendencies among the different catalysts studied and there is not any significant change in the mechanisms due to the modification of the HZSM-5 zeolite with KOH or H_3PO_4. Coke content in the deactivated catalyst (Fig. 6b) follows the same tendency as BTX selectivity.

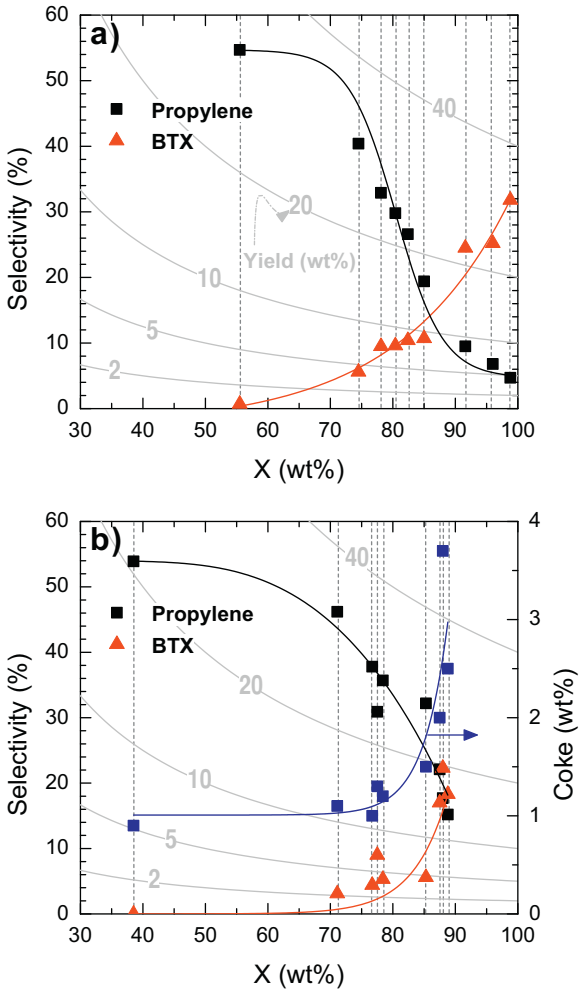

Fig. 6. Correlation of propylene and BTX selectivity with the butene conversion (X) at (a) 0 h and (b) 5 h on stream. In the latter graph, coke content is also represented.

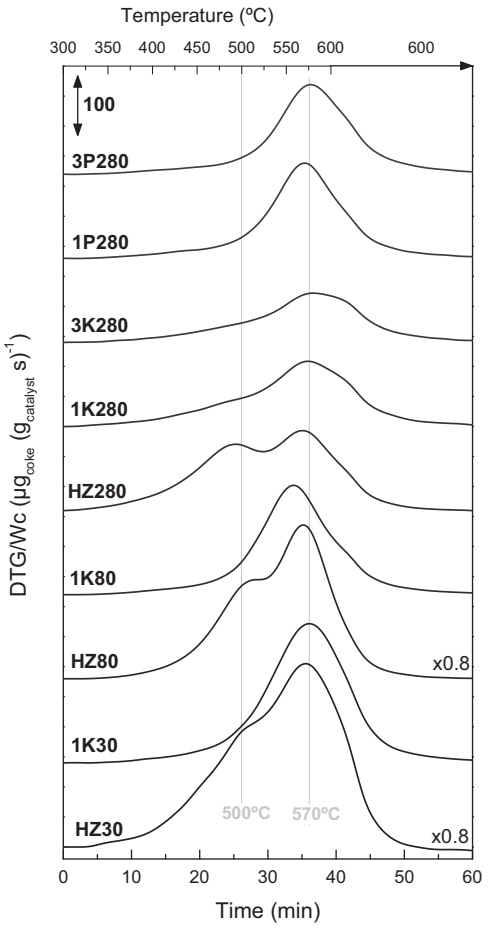

Fig. 7. TPO of coke (differential thermogravimetry per gram of catalysts) deposited on the catalysts of unmodified and modified MFI zeolites after 5 h on stream.

On the other hand, the evolution of propylene selectivity is reverse to that of BTX so that it decreases at higher conversion values. These observations indicate that 1-butene conversion follows a sequential pathway of oligomerization-cracking to form propylene and ethylene, subsequent aromatization and final condensation of aromatics into coke (Fig. 6), as previously demonstrated [38]. In terms of stability, K- and P-modified zeolites are similar to their corresponding unmodified counterparts, however a lower deposition by coke is observed (<2.0 wt%) for the modified zeolites. This effect is more significant at low SiO_2/Al_2O_3 ratios. In the case of 3K280 catalysts, a more significant conversion decay is observed; −31% compared to −6% for the HZ280 catalyst, which is attributed to the low amount of acid sites with weak acidity that are more sensitive to coke deactivation.

Fig. 7 shows the TPO profiles corresponding to the combustion of the coke deposited on the unmodified and modified catalysts after 5 h time on stream. Two types of coke are identified: (i) coke I, burning off at 500 °C and; (ii) coke II burning off at 570 °C. In a previous work [66], we have identified the nature of these types of coke by *in-situ* FTIR analysis concluding the more aliphatic and disordered nature of coke I and more condensed and structured aromatic nature of coke II. Besides, coke II has a strong contribution of coke deposited in the interior of the zeolite crystals and it is formed firstly, whereas coke I is located more externally in the mesopores of the zeolite or the matrix [45,66,71]. The amount and the fact that coke I is present demonstrates that HZ30, HZ80 and HZ280 catalysts are in stage of higher deactivation or coke growth as compared to the rest of catalysts, that only show coke II. The modification of MFI zeolite with H_3PO_4 and KOH decrease the rate of coke formation and growth.

The trends of selectivity and deactivation observed here for the catalysts of unmodified and modified MFI catalysts (Table 5) have been previously described using zeolites with lower SiO_2/Al_2O_3 ratio. Our results point to the outstanding performance of high-silica MFI zeolite for the cracking of 1-butene pursuing the maximum selectivity of propylene, so we have decided to focus on this HZ280 zeolite and its modified counterparts. Historically, the improvement of modified zeolites over unmodified ones has been rationalized in terms of the neutralization of Brönsted acid sites, particularly strong ones [46,72]. However, our characterization results show that different features are interconnected with Brönsted acidity, dealumination and desilication. In view of these premises, we performed a sensitivity analysis followed by a regression analysis of the most sensitive features of the MFI zeolite.

3.3. Correlation between catalytic features and performance

This Section aims correlating the structural, physical and acid properties of the MFI zeolite with $SiO_2/Al_2O_3 = 280$ with their kinetic performance in order to identify the most controlling features of the catalysts. The 19 catalyst properties (independent or input variables, I) of this set of 5 catalysts (HZ280, 1K280, 3K280, 1P280 and 3P230) have already been shown in Tables 1–3, whereas the 19 catalytic performance variables (dependent or output variables, O) have been shown in Tables 4–5. A complete list of the

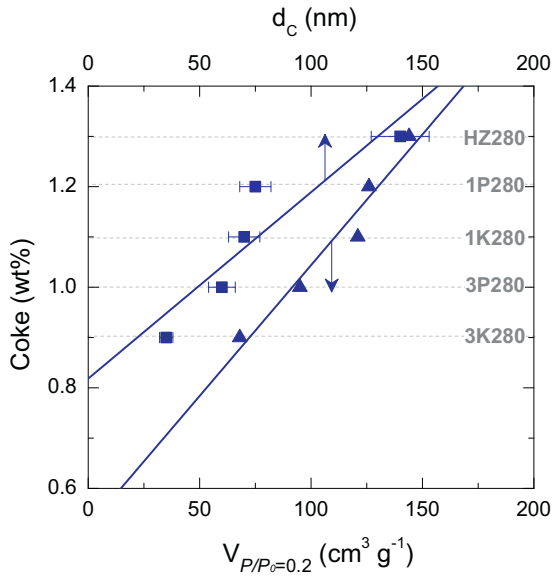

Fig. 8. Correlation between the coherent diffraction crystal size (d_c) and volume of N_2 adsorbed at $P/P_0 = 0.2$ ($V_{P/P0=0.2}$) with the amount of coke deposited on the catalyst after 5 h on stream for the 280 catalyst family.

variables is summarized in Tables S1–S2 of the Supplementary material. We followed the following method for selecting the most important variables: (1) calculate the sensitivity factors or elasticity coefficients (Ω) of each pair of i input and j output [73]:

$$\Omega_k = |\log_{10}\left(\frac{\bar{I}_i}{\bar{O}_j}\frac{|\Delta\bar{O}_j|}{|\Delta\bar{I}_i|}\right)| \quad (6)$$

where Δ refers to the maximum difference of values. We chose pairs (k) with $\Omega_k > 1$ as arbitrary criteria, (2) we excluded variables that do not vary significantly within the experimental range of this study:

$$|\frac{I_i^{max} - I_i^{min}}{\bar{I}_i}| < 0.8, |\frac{O_i^{max} - O_i^{min}}{\bar{O}_i}| < 0.8 \quad (7)$$

where the variables I^{max}, I^{min} and $\bar{I}$ refer to the maximum, minimum and mean of the input or output variable. (3) The selected input-output pairs for nonlinear regression analysis using *nlinfit* in MATLAB™, using potential models. The final selection of the controlling input–output pair corresponds to the minimal sum of Averaged Sum of Squared Residuals (ASSR):

$$\text{ASSR} = \frac{\sum_{j=1}^{n}(O_j|_{exp} - O_j|_{calc})^2}{\sum_{j=1}^{n}(O_j|_{exp})^2} \quad (8)$$

Tables in the Supplementary material summarize the elasticity coefficients (Table S1) and ASSR (Table S2). These tables show that the most sensitive correlations and best fittings correspond to the pairs acid strength-conversion, acid strength-selectivity, d_c-coke and $V_{P/P0=0.2}$-coke. Indeed, Fig. 8 shows the most sensitive correlations using linear regression analysis; coke formation is correlated with the crystal size of the zeolite and the volume of micropores ($V_{P/P0=0.2}$) of the catalysts. The absolute values of crystal size and volume of micropores should be taken with care, considering the way they have been calculated. Nevertheless, the observed correlation still holds and indicates that the deactivation by coke is strongly influenced by the outward diffusion of coke precursors formed within the micropores of the catalyst, which easily evacuates zeolites that have been desilicated. Xu et al. [13] have found that the deactivation of unmodified and modified MFI zeolite is not a function of acidity in the cracking of 1-butene, which could be associated to their absence of desilication. Interestingly, we could not correlate neither by linear nor nonlinear regression models the coke content with acidity or the loss of activity. However we observed these kinds of correlations when comparing unmodified zeolites (HZ30, HZ80 and HZ280). This indicates that acidity plays a significant role in deactivation when considering sets of catalysts with very different nature and strength of acid sites, whereas desilication seems to control deactivation within unmodified and modified high-silica zeolites (HZ280).

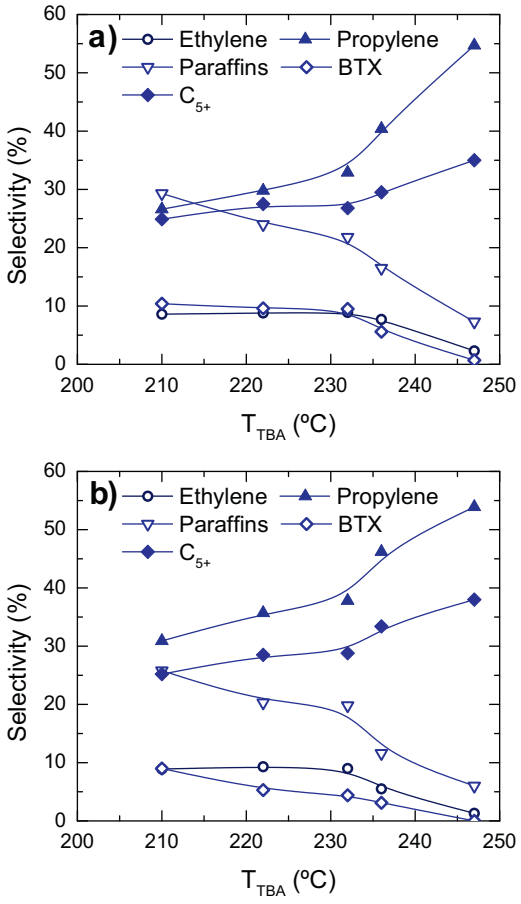

Fig. 9. Correlation of product selectivity with the acid strength of the catalysts measured by the temperature of maximum t-BA desorption-cracking rate (T_{TBA}) for the 280 catalyst family: (a) 0 h and (b) 5 h on stream.

Fig. 9 shows the correlation of acid strength (measured by temperature of maximum t-BA desorption-cracking rate, T_{TBA}) with the product selectivity of the reaction after 0 h (Fig. 9a) and 5 h of stream (Fig. 9b). An increase in the acid strength favors light paraffin and BTX formation, whereas propylene and C_{5+} (mainly olefinic) selectivity notably decreases. Strongest acid sites ($T_{TBA} < 210\,^{\circ}C$) enhance both hydrogen transfer and aromatization reactions, thus enhancing the formation of aromatics and paraffins. On the contrary, weakest acid sites ($T_{TBA} > 225\,^{\circ}C$) promote oligomerization reaction yielding mainly propylene. These results are in good agreement with these published recently by Lin et al. [40]. Fig. S3 of the Supplementary material provides additional data of the correlation of selectivity of products and conversion of 1-butene. It should be mentioned that with an industrial perspective, the fraction C_{5+} should be recirculate to the cracking unit for boosting the entire performance of the process.

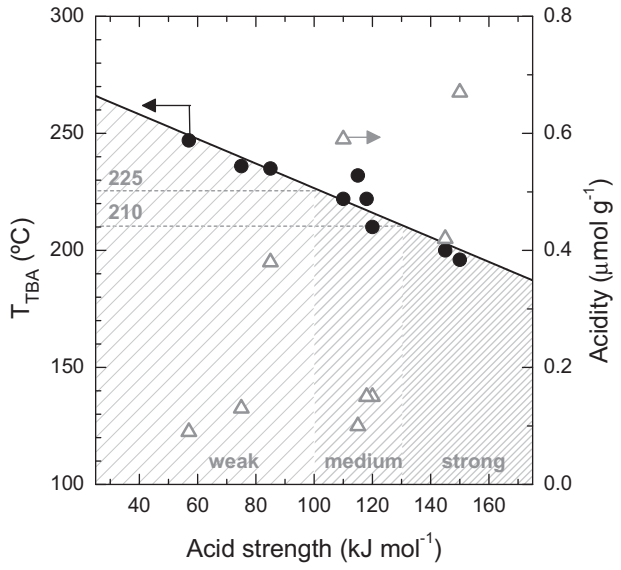

Fig. 10. Correlation of acidic strength and temperature of maximum t-BA desorption-cracking rate (T_{TBA}) and acidity of the catalyst. Areas of strong, medium and weak acidities are represented by different density and width of lines.

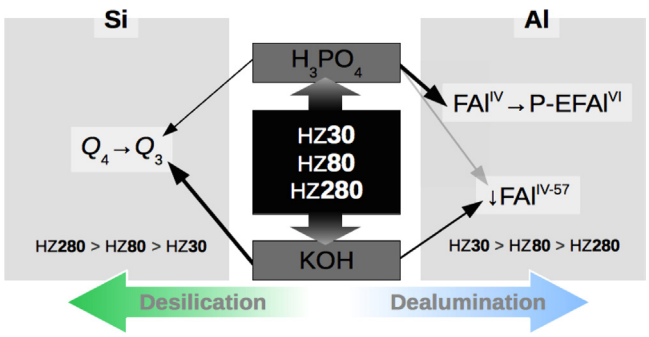

Fig. 11. Diagram of results obtained in this work, interpreted from the modification of MFI zeolite with KOH or H_3PO_4.

On view of our results, a suitable balance between the acid strength is required for balancing conversion and selectivity of propylene. Moreover, deactivation should be considered as another decisive factor, and coke deposition is minimized for the KOH treated zeolites that has suffered desilication, reducing the diffusion length of coke precursors and helping the outward diffusion of these species. A good compromise between all these factors is obtained for the 1K280 catalyst.

4. Discussion

The results obtained here allows correlating the acid strength obtained by (a) the acid strength-heat dissipated during isothermal adsorption of t-BA at 150 °C- and (b) the desorption temperature of t-BA (T_{TBA}). Fig. 10 shows that this correlation has a linear dependency and enable pointing the limits of strong, medium and weak acidity: > 130 kJ $(mol_{t\text{-}BA})^{-1}$ or T_{TBA} < 210 °C, 100–130 kJ $(mol_{t\text{-}BA})^{-1}$ or 210 < T_{TBA} < 225 °C, and < 100 kJ $(mol_{t\text{-}BA})^{-1}$ or T_{TBA} > 225 °C, respectively. This kind of correlation has been investigated for NH_3 extensively, however is better correlated using t-BA. As shown in Fig. 10, the number of acid sites is not linearly dependent with the acid strength.

Fig. 11 aims to rationalize the results obtained here; we have modified MFI zeolites of different SiO_2/Al_2O_3 ratios (30, 80 and 280) with H_3PO_4 and KOH, obtaining modified zeolites in the following manner.

Al environment: K-modified MFI zeolites show significant drop of accessible framework Al, as demonstrated by the NMR band ratio (FAl^{IV-57}/FAl^{IV-54}, Table 3), and the extent of this drop is a function of the initial SiO_2/Al_2O_3 ratio. This drop of accessible FAl^{IV} derives into neutralization of the most acidic Brönsted acid sites of the zeolites as proved by TPD of t-BA (Fig. 5). P-modified MFI zeolites show a significant conversion of FAl^{IV} sites into P-$EFAl^{VI}$ sites. Despite this significant conversion of more than 50%, we do not observe a proportional drop in the acidity or in the conversion of the modified catalysts. This result indicates that P-$EFAl^{VI}$ sites participate in the acidic adsorption of t-BA and in the reactions involved during the conversion of 1-butene.

Si environment: both K- and P-modified zeolites show significant desilication which is greater for the MFI zeolites with the higher SiO_2/Al_2O_3 ratio and for the K-modified catalysts, as deduced by the chemical shift of the ^{29}Si NMR bands. This result indicates that desilication is favored by increasing the amount of the reactants involved: FSi and alkali media.

Despite the fact that the values of crystal size and micropore volume are not completely reliable, our results show that coke content is sensitive to the extent of desilication with KOH, and therefore to the environment of Si. Our results show that the Al environment is greatly modified with H_3PO_4 (Table 2), whereas the number of acid sites and the acid strength is greatly modified with KOH. Nevertheless both modifications change the environments of Si and Al simultaneously. Thus and according to the results, H_3PO_4 treatment expands the lifetime of the MFI zeolite catalyst whereas KOH treatment increases propylene selectivity. A good compromise of low catalyst deactivation and high propylene production is obtained for the 1K280 catalyst.

5. Conclusions

We have studied the parameters of the MFI zeolite governing selectivity and deactivation performance during the cracking of 1-butene. Studied zeolites include different SiO_2/Al_2O_3 ratios and modification degree with KOH and H_3PO_4.

We have obtained a linear correlation between the acid strengths obtained by the heat dissipated during isothermal adsorption of tert-butylamine and the temperature- programmed desorption (TPD) of the same base, using MFI catalyst with different SiO_2/Al_2O_3 ratio or modification procedures. This result enables a fast characterization of this critical catalytic feature; acid strength.

The catalytic performance, in terms of a high propylene selectivity and slow deactivation by coke, is strongly improved by using high silica zeolites (SiO_2/Al_2O_3 ratio = 280) modified with of K or P. Nevertheless, the conversion of 1-butene is significantly decreased in the same trend. A good balance of low catalyst deactivation and high propylene production is obtained for the 1K280 catalyst.

Our work supports the general concern that the acidity plays a significant role in 1-butene cracking when comparing zeolites of different SiO_2/Al_2O_3 ratio: Increasing conversion and decreasing propylene selectivity for zeolites with lower SiO_2/Al_2O_3 ratio. On the other hand, the main contribution of this work deals with the clarification of the controlling features of the high silica MFI zeolites, which are the most promising catalysts for propylene production. This has been elucidated using a combination of sensitivity and regression analysis between the catalytic features and their performance. In this sense and with the unmodified and modified high silica MFI zeolites (SiO_2/Al_2O_3 = 280), acid strength is the key factor controlling conversion of 1-butene and selectivity of propylene. Besides, the decrease in the diffusion length of the coke precursors is the key factor controlling coke deactivation and the

lifetime of the catalyst, as it favors the outward diffusion of coke precursors.

Acknowledgements

The financial support of this work was undertaken by the Ministry of Economy and Competitiveness (MINECO) of the Spanish Government (CTQ2013-46172-P, CTQ2010-19623 and CTQ2010-19188 projects), FEDER funds and by the University of the Basque Country (UFI 11/39). E. Epelde (BFI08.122) is grateful for her Ph.D. grant from the Department of Education, University and Research of the Basque Country and for the University of the Basque Country. The technical and human support provided by SGIker (UPV/EHU, MICINN, GV/EJ, ESF) is gratefully acknowledged, particularly to Aitor Larrañaga.

References

[1] M. Ibáñez, M. Artetxe, G. Lopez, G. Elordi, J. Bilbao, M. Olazar, P. Castaño, Appl. Catal. B: Environ. 148–149 (2014) 436–445.
[2] P. Castaño, G. Elordi, M. Olazar, J. Bilbao, ChemCatChem 4 (2012) 631–635.
[3] P. Castaño, G. Elordi, M. Ibañez, M. Olazar, J. Bilbao, Catal. Sci. Technol. 2 (2012) 504–508.
[4] N. Rahimi, R. Karimzadeh, Appl. Catal. A: Gen. 398 (2011) 1–17.
[5] X. Zhu, S. Liu, Y. Song, L. Xu, Appl. Catal. A: Gen. 288 (2005) 134–142.
[6] A.S. Al-Dughaither, H. de Lasa, Ind. Eng. Chem. Res. 53 (2014) 15303–15316.
[7] G. Elordi, M. Olazar, M. Artetxe, P. Castaño, J. Bilbao, Appl. Catal. A: Gen. 415–416 (2012) 89–95.
[8] G.L. Woolery, G.H. Kuehl, Zeolites 19 (1997) 288–296.
[9] L.H. Ong, M. Dömök, R. Olindo, A.C. van Veen, J.A. Lercher, Microporous Mesoporous Mater. 164 (2012) 9–20.
[10] M. Niwa, S. Sota, N. Katada, Catal. Today 185 (2012) 17–24.
[11] E.F. Sousa-Aguiar, F.E. Trigueiro, F.M.Z. Zotin, Catal. Today 218–219 (2013) 115–122.
[12] J. Liu, C. Zhang, Z. Shen, W. Hua, Y. Tang, W. Shen, Y. Yue, H. Xu, Catal. Commun 10 (2009) 1506–1509.
[13] R.-f. Xu, J.-x. Liu, C.-c. Liang, W.-h. Jia, F.-f. Li, H.-c. Guo, J. Fuel Chem. Technol. 39 (2011) 449–454.
[14] Y. Jiao, C. Jiang, Z. Yang, J. Liu, J. Zhang, Microporous Mesoporous Mater. 181 (2013) 201–207.
[15] Y. Li, D. Liu, S. Liu, W. Wang, S. Xie, X. Zhu, L. Xu, J. Nat. Gas Chem. 17 (2008) 69–74.
[16] T. Blasco, A. Corma, J. Martínez-Triguero, J. Catal. 237 (2006) 267–277.
[17] M. Göhlich, W. Reschetilowski, S. Paasch, Microporous Mesoporous Mater. 142 (2011) 178–183.
[18] S.M. Cabral de Menezes, Y.L. Lam, K. Damodaran, M. Pruski, Microporous Mesoporous Mater. 95 (2006) 286–295.
[19] K. Damodaran, J.W. Wiench, S.M. Cabral de Menezes, Y.L. Lam, J. Trebosc, J.P. Amoureux, M. Pruski, Microporous Mesoporous Mater. 95 (2006) 296–305.
[20] J.A. Van Bokhoven, D.C. Koningsberger, P. Kunkeler, H. Van Bekkum, A.P.M. Kentgens, J. Am. Chem. Soc. 122 (2000) 12842–12847.
[21] D. Liu, W.C. Choi, C.W. Lee, N.Y. Kang, Y.J. Lee, C.-H. Shin, Y.K. Park, Catal. Today 164 (2011) 154–157.
[22] M. Derewinski, P. Sarv, X. Sun, S. Müller, A.C. Van Veen, J.A. Lercher, J. Phys. Chem. C 118 (2014) 6122–6131.
[23] N. Xue, R. Olindo, J.A. Lercher, J. Phys. Chem. C 114 (2010) 15763–15770.
[24] S.P.R. Katikaneni, J.D. Adjaye, R.O. Idem, N.N. Bakhshi, Ind. Eng. Chem. Res. 35 (1996) 3332–3346.
[25] E. Epelde, A.G. Gayubo, M. Olazar, J. Bilbao, A.T. Aguayo, Chem. Eng. J. 251 (2014) 80–91.
[26] D. Tzoulaki, A. Jentys, J. Pérez-Ramírez, K. Egeblad, J.A. Lercher, Catal. Today 198 (2012) 3–11.
[27] L. Zhao, J. Gao, C. Xu, B. Shen, Fuel Process. Technol. 92 (2011) 414–420.
[28] J. Kim, M. Choi, R. Ryoo, J. Catal. 269 (2010) 219–228.
[29] J.S. Jung, J.W. Park, G. Seo, Appl. Catal. A: Gen. 288 (2005) 149–157.
[30] H. Konno, T. Okamura, T. Kawahara, Y. Nakasaka, T. Tago, T. Masuda, Chem. Eng. J. 207–208 (2012) 490–496.
[31] E. Epelde, A. Gayubo, M. Olazar, J. Bilbao, A. Aguayo, Ind. Eng. Chem. Res. 53 (2014) 4614–4622.
[32] N. Xue, X. Chen, L. Nie, X. Guo, W. Ding, Y. Chen, M. Gu, Z. Xie, J. Catal. 248 (2007) 20–28.
[33] P. Castaño, J. Ruiz-Martinez, E. Epelde, A.G. Gayubo, B.M. Weckhuysen, ChemCatChem 5 (2013) 2827–2831.
[34] J. Plotkin, Catal. Today 106 (2005) 10–14.
[35] E. Mazoyer, K.C. Szeto, N. Merle, S. Norsic, O. Boyron, J.-M. Basset, M. Taoufik, C.P. Nicholas, J. Catal. 301 (2013) 1–7.
[36] A. Coelho, G. Caeiro, M.A.N.D.A. Lemos, F. Lemos, F. Ramôa Ribeiro, Fuel 111 (2013) 449–460.
[37] J.S. Buchanan, J.G. Santiesteban, W.O. Haag, J. Catal. 158 (1996) 279–287.
[38] E. Epelde, A.T. Aguayo, M. Olazar, J. Bilbao, A.G. Gayubo, Ind. Eng. Chem. Res. 53 (2014) 10599–10607.
[39] P. Sazama, J. Dedecek, V. Gábová, B. Wichterlová, G. Spoto, S. Bordiga, J. Catal. 254 (2008) 180–189.
[40] L. Lin, C. Qiu, Z. Zhuo, D. Zhang, S. Zhao, H. Wu, Y. Liu, M. He, J. Catal. 309 (2014) 136–145.
[41] T.R. Koyama, Y. Hayashi, H. Horie, S. Kawauchi, A. Matsumoto, Y. Iwase, Y. Sakamoto, A. Miyaji, K. Motokura, T. Baba, Phys. Chem. Chem. Phys. 12 (2010) 2541–2554.
[42] A. Saltelli, M. Ratto, S. Tarantola, F. Campolongo, Chem. Rev. (Washington, DC, U. S.) 112 (2012) PR1–PR21.
[43] N. Agarwal, M.A. Sanchez-Castillo, R.D. Cortright, R.J. Madon, J.A. Dumesic, Ind. Eng. Chem. Res. 41 (2002) 4016–4027.
[44] A. Gutiérrez, J.M. Arandes, P. Castaño, A.T. Aguayo, J. Bilbao, Energy Fuels 25 (2011) 3389–3399.
[45] E. Epelde, A.T. Aguayo, M. Olazar, J. Bilbao, A.G. Gayubo, Appl. Catal. A: Gen. 479 (2014) 17–25.
[46] A.T. Aguayo, A.G. Gayubo, R. Vivanco, M. Olazar, J. Bilbao, Appl. Catal. A: Gen. 283 (2005) 197–207.
[47] L.E. Sandoval-Díaz, J.A. González-Amaya, C.A. Trujillo, Microporous Mesoporous Mater. 215 (2015) 229–243.
[48] G. Caeiro, P. Magnoux, J.M. Lopes, F. Ramôa Ribeiro, S.M.C. Menezes, A.F. Costa, H.S. Cerqueira, Appl. Catal. A: Gen. 314 (2006) 160–171.
[49] A.W. Burton, K. Ong, T. Rea, I.Y. Chan, Microporous Mesoporous Mater. 117 (2009) 75–90.
[50] P. Morales-Pacheco, J.M. Domínguez, L. Bucio, F. Alvarez, U. Sedran, M. Falco, Catal. Today 166 (2011) 25–38.
[51] M. Hunger, Microporous Mesoporous Mater. 82 (2005) 241–255.
[52] J. Kanellopoulos, A. Unger, W. Schwieger, D. Freude, J. Catal. 237 (2006) 416–425.
[53] H. Koller, M. Weiß, 2012, pp. 189–228.
[54] G. Zhao, J. Teng, Z. Xie, W. Jin, W. Yang, Q. Chen, Y. Tang, J. Catal. 248 (2007) 29–37.
[55] J. Zhuang, D. Ma, G. Yang, Z. Yan, X. Liu, X. Han, X. Bao, P. Xie, Z. Liu, J. Catal. 228 (2004) 234–242.
[56] J. Kučera, P. Nachtigall, Microporous Mesoporous Mater. 85 (2005) 279–283.
[57] S.M. Maier, A. Jentys, J.A. Lercher, J. Phys. Chem. C 115 (2011) 8005–8013.
[58] P. Sarv, C. Fernandez, J.P. Amoureux, K. Keskinen, J. Phys. Chem. 100 (1996) 19223–19226.
[59] J.A. Ke, I. Wang, Mater. Chem. Phys. 68 (2001) 157–165.
[60] C.A. Fyfe, Y. Feng, H. Grondey, Microporous Mater. 1 (1993) 401–411.
[61] V.L. Barrio, P.L. Arias, J.F. Cambra, M.B. Güemez, B. Pawelec, J.L.G. Fierro, Appl. Catal. A: Gen. 242 (2003) 17–30.
[62] J.C. Groen, J. Pérez-Ramírez, Appl. Catal. A: Gen. 268 (2004) 121–125.
[63] G. Jiang, L. Zhang, Z. Zhao, X. Zhou, A. Duan, C. Xu, J. Gao, Appl. Catal. A: Gen. 340 (2008) 176–182.
[64] M. Ogura, M. Matsukata, in: J. García-Martínez, K. Li, M.E. Davis (Eds.), Mesoporous Zeolites: Preparation, Characterization and Applications, Wiley-VCH, 2015, pp. 259–294.
[65] S. Mitchell, N.L. Michels, K. Kunze, J. Pérez-Ramírez, Nat. Chem. 4 (2012) 825–831.
[66] E. Epelde, M. Ibañez, A.T. Aguayo, A.G. Gayubo, J. Bilbao, P. Castaño, Microporous Mesoporous Mater. 195 (2014) 284–293.
[67] X. Zhu, S. Liu, Y. Song, L. Xu, Catal. Lett. 103 (2005) 201–210.
[68] P. Castaño, A.G. Gayubo, B. Pawelec, J.L.G. Fierro, J.M. Arandes, Chem. Eng. J. 140 (2008) 287–295.
[69] G.L. Zhao, J.W. Teng, Z. Xie, W.M. Yang, Q.L. Chen, Y. Tang, Stud. Surf. Sci. Catal. 170 (2007) 1307–1312.
[70] J. Dědeček, D. Kaucky, B. Wichterlova, Chem. Commun. (2001) 970–971.
[71] M. Ibañez, B. Valle, J. Bilbao, A.G. Gayubo, P. Castaño, Catal. Today 195 (2012) 106–113.
[72] M. Guisnet, L. Costa, F. Ramôa Ribeiro, J. Mol. Catal. A: Chem. 305 (2009) 69–83.
[73] A. Saltelli, M. Ratto, S. Tarantola, F. Campolongo, Chem. Rev. (Washington, DC, U. S.) 112 (2012) PR1–PR21.